Inorganic Chemistry

ARTICLE

pubs.acs.org/IC

An Incommensurately Modulated Structure of η'-Phase of $Cu_{3+x}Si$ Determined by Quantitative Electron Diffraction Tomography

Lukáš Palatinus,*[,†] Mariana Klementová,[†,§] Vladislav Dřínek,[‡] Markéta Jarošová,[†] and Václav Petříček[†]

[†]Institute of Physics of the AS CR, v.v.i., Na Slovance 2, 182 21 Prague, Czechia

[‡]Institute of Chemical Process Fundamentals of the AS CR, v.v.i., Rozvojová 135, 165 02 Prague 6, Czechia

[§]Institute of Inorganic Chemistry of the AS CR, v.v.i., 250 68 Husinec-Řež 1001, Czechia

Supporting Information

ABSTRACT: The diffraction data of η'-Cu_{3+x}(Si,Ge) were collected by 3D quantitative electron diffraction tomography on a submicrometer-sized sample, and the structure was solved by the charge-flipping algorithm in superspace. It is shown that the structure is trigonal, and it is incommensurately modulated with two modulation vectors $q_1 = (\alpha, \alpha, 1/3)$ and $q_2 = (-2\alpha, \alpha, 1/3)$, superspace group $P\bar{3}1m(\alpha, \alpha, 1/3)000(-2\alpha, \alpha, 1/3)000$. The modulation functions of some atoms are very complicated and reach amplitudes comparable with the unit cell dimensions. The modulated structure can be described as sheets of Cu clusters separated by honeycomb layers of mixed Si/Ge positions. The shape of the Cu clusters in the sheets strongly varies with the modulation phase, and the predominant form is an icosahedron. The striving of the Cu layers to form icosahedral clusters is deemed to be the main driving force of the modulation. The combination of methods used in this work can be applied to other structures that are difficult to crystallize in large crystals and opens new perspectives, especially for investigations of aperiodic or otherwise complex metallic alloys.

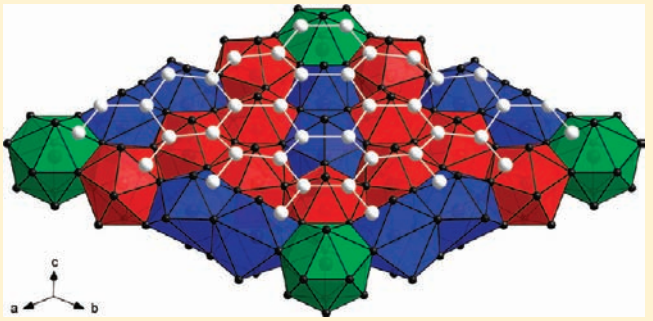

INTRODUCTION

Understanding the atomic arrangements in crystals is the cornerstone of most of the solid-state physics and chemistry. The number of crystal structures deposited in various databases approaches one million. Despite of the tremendous progress crystallography has made over the past decades, many interesting structures have remained unsolved. The usual reason is that the material is hard or impossible to crystallize in crystals large enough for single-crystal study, and the structure is too complex to be solved by powder diffraction techniques. Metallic alloys represent a prominent class of such materials. It is well-known that metallic alloys have a tendency to form very complex structures including some of the largest inorganic structures ever observed,[1] quasicrystals and their approximants.[2] The scientific literature is abundant with reports on complex diffraction patterns of metallic alloys, often indicating nonperiodic (incommensurately modulated or quasicrystalline) features. Many of these structures remain unsolved, or only a tentative structural model is proposed on the basis of qualitative considerations.

Cu_3Si is a prominent example of this class of compounds. Cu_3Si is used as a catalyst for the production of technologically highly important chlorosilanes, an intermediate compound in the production of ultrapure silicon for the semiconductor industry.[3] Copper silicides and copper germanides have also been studied as materials for applications as contacts and interconnects in Si and Ge−Si electronic devices.[4,5] A large body of work has been published on the physical and chemical properties of Cu_3Si;[4−11] on the growth mechanism and morphology of Cu_3Si nanoparticles in silicon;[12−16] and on the formation of epitaxial layers of Cu_3Si grown on oriented Si, Ge, or Si−Ge substrates.[17−19]

In striking contrast to the detailed understanding of the properties of Cu_3Si, very little is known about its structure. Cu_3Si is one of three stable binary phases in the system Cu−Si. It is better characterized by the formula $Cu_{3+x}Si$, and its room-temperature modification, η''-Cu_3Si, transforms upon heating to two high-temperature phases, η'-Cu_3Si and η-Cu_3Si.[6] The first structural investigation in 1931[20] using powder X-ray diffraction revealed a complex superstructure. In 1978, Solberg[21] investigated precipitates of Cu_3Si in silicon using electron diffraction and concluded that the structure is based on a body-centered cubic structure and that the superstructure is formed by chemical ordering of copper and silicon atoms. This model had been taken for granted and was referenced in all studies of Cu_3Si, until in 2007, Wen and Spaepen[22] demonstrated that the model proposed by Solberg is wrong. A new structural model for the high-temperature η-Cu_3Si was suggested with lattice parameters a = 4.06 Å and c = 7.33 Å and a trigonal symmetry of $P\bar{3}m1$.

Received: January 17, 2011
Published: March 25, 2011

The superstructures in the low-temperature phases were again tentatively explained by the chemical ordering and a special stacking sequence of the η-Cu_3Si units. The same structural model for η-Cu_3Si has been independently proposed by Mattern and co-workers[23] using an X-ray powder diffraction pattern.

Some of the first crystallographic data for the intermetallic compounds of the Cu−Ge system was provided by Schubert and Brandauer;[24] later it was completed by Huaiying.[25] It is reported that Cu_3Ge has a hexagonal structure with lattice parameters a = 4.17 Å and c = 4.92 Å at a high temperature and an orthorhombic structure with lattice parameters a = 4.202 Å, b = 4.553 Å, and c = 2.645 Å at a low temperature. Lattice parameters depend on the germanium content. However, Nowotny and Bachmayer[26] report a monoclinic distortion of the orthorhombic cell, with cell parameters a = 2.631 Å, a = 4.200 Å, a = 4.568 Å, and β = 89.68° and a distorted *hcp* structure where germanium and copper occupy identical crystallographic positions. Monoclinic distortion of Cu_3Ge is also reported by Krusin-Elbaum and Aboelfotoh.[27]

In this report, we present a structural description of η'-Cu_3Si. Using a crystal of submicrometer size, we show that the structure is incommensurately modulated, and that the observed long-period superstructure is not due to chemical ordering or stacking order but due to extreme positional modulations within the structure. This work shows that structure models proposed on the basis of a qualitative evaluation of the electron diffraction pattern may be incorrect. The method that we used is general and can be applied to other structures and opens a new perspective for studies of complex, especially aperiodic arrangements of metallic alloys and other challenging structures.

Incommensurate structures are commonly described in superspace with as many dimensions as the number of integers necessary to index the diffraction pattern. The real structure is then obtained as a special section of the superspace structure. A sound and comprehensive introduction to the concept of superspace is presented by Wagner and Schönleber.[28] The interested reader can find full details in the recent book *Incommensurate Crystallography*.[29]

The structure could be solved only thanks to the combination of several emerging methodological advances. The diffraction data were collected by 3D diffraction tomography combined with precession electron diffraction. 3D diffraction tomography is a technique commonly used in X-ray diffraction, when a crystal is rotated around a specific axis in small steps, and in each step the diffraction pattern is recorded. In electron diffraction, only recently have serious attempts been made to automatize the procedure.[30,31] However, useful data can be collected also with manual tilting of the sample, and this technique was also used in this work. The diffraction patterns were collected by the precession diffraction method.[32] In this method, the beam performs a precessing motion around a surface of a cone with a vertex at the sample. This precessing motion is compensated under the sample, so that the resulting diffraction pattern forms spots and not circles. Precession electron diffraction was shown to partially suppress the dynamical diffraction effects occurring in electron diffraction.[33−36] Thanks to this method, the collected diffraction intensities can be, in contrast to classical SAED diffraction patterns, used to solve the crystal structure by *ab initio* phasing methods developed in the context of X-ray crystallography.

Aperiodic structures also represent a special challenge for the structure solution. The era of routine *ab initio* structure solution of aperiodic structures from X-ray diffraction data started only in the year 2004, when the charge flipping algorithm was published[37,38] and generalized to superspace.[39] The charge flipping algorithm has been applied to a wide range of crystallographic problems since its publication, including structure solution from electron diffraction data.[40,41] In this work, the charge flipping algorithm was, to our knowledge, used for the first time to solve an aperiodic structure from precession electron diffraction data.

EXPERIMENTAL AND DATA PROCESSING

The material was synthesized by Low Pressure Chemical Vapor Deposition (CVD) from organometallic precursors hexamethyldigermane ($Ge_2(CH_3)_6$, Aldrich, tech.) and ethylsilane ($SiH_3C_2H_5$, our stock) deposited on a copper foil substrate (0.1 mm, 99.99%). The substrate was cleaned in an ultrasonic bath with acetone prior to the experiment and placed in a quartz tube. The tube was evacuated to a pressure of 10^{-4} Pa and placed in an oven heated to 500 °C. Then, the gaseous mixture was continuously injected into the tube and simultaneously exhausted. Partial pressures of hexamethyldigermane and ethylsilane were 100 and 50 Pa, respectively. After 1.5 h, the injection of gases was interrupted, and the oven was switched off. The substrates were kept under vacuum conditions until the temperature inside the tube decreased below 60 °C. The experiment yielded nanoplatelets with lateral dimensions of several micrometers, but with a thickness of only about 40 nm (Figure 1a).

An initial investigation of the samples was performed on a JEOL JEM-3010 transmission electron microscope with a LaB_6 cathode operating at 300 kV. Images were recorded on a Gatan CCD camera with a resolution of 1024 × 1024 pixels using the Digital Micrograph software package. Samples were transferred onto a holey carbon-coated nickel grid by brushing the grid against the copper substrate containing the deposit. First, oriented diffraction patterns of several platelets were collected (Figure 1b). These patterns revealed an incommensurately modulated structure. The complex diffraction pattern is not a consequence of twinning, but it stems from one phase. This is evidenced by high-resolution TEM images (Figure 1c,d), which also confirm the incommensurate structure of the phase. An EDX analysis (JXA-733, JEOL with energy-dispersive spectrometer KEVEX) revealed a composition of 76.1(8) atom % Cu, 11.7(9) atom % Si, and 12.2(7) atom % Ge. This corresponds to the formula Cu_{3+x}(Si,Ge) with $x \approx 0.19$ and a Si/Ge ratio of 1:1 within the experimental error. Comparison with the published diffraction patterns of $Cu_{3+x}Si$[22] shows that the phase is isostructural with the η'-phase of $Cu_{3+x}Si$. Therefore, this study applies to the ternary compound Cu_{3+x}(Si,Ge) as well as to the binary alloy $Cu_{3+x}Si$. For this reason, if we refer to general properties of the structure, we will refer to it as $Cu_{3+x}Si$, and only if our specific sample is discussed, will we explicitly mention the Ge contents.

The data collection for the structural investigation was conducted on a Philips CM120 transmission electron microscope with a LaB_6 cathode operating at 120 kV. The microscope is equipped with a SpinningStar (NanoMegas) precession device for application of the precession electron diffraction (PED),[32] and with a CCD Camera Olympus SIS Veleta with 14 bit dynamical range. The precession electron diffraction was used so that the dynamical diffraction effects present in standard electron diffraction are suppressed to as large of an extent as possible. A small, homogeneous part of one platelet (Figure 1a) was selected for data collection of a three-dimensional diffraction pattern. The crystal was not oriented along a special zone axis prior to the data collection but was intentionally left in a random orientation. The precession semiangle was set to 1°. The crystal was tilted in steps of 1° around the main tilt axis of the sample holder, and in each step two diffraction patterns were collected, one with 200 ms exposure and the other with 5 s exposure. The double exposure was used to accurately collect the intensities of both the strong and the weak reflections. A total of 82 pairs of patterns were collected in the interval −31° to +50°. At higher tilts, the crystal was shaded by the sample holder.

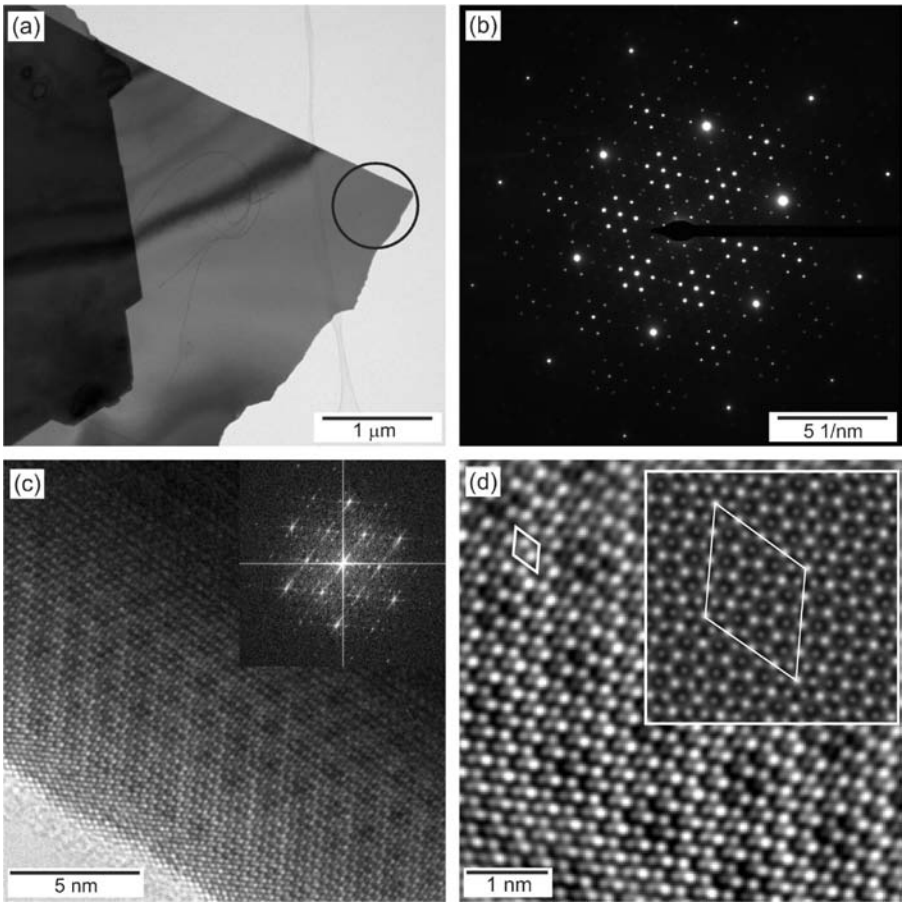

Figure 1. (a) Crystal used for the collection of the diffraction data. The black circle shows the region selected by the selected area aperture. (b) A SAED diffraction pattern of the zone [001]. (c) High-resolution TEM image, view along [001]. (d) A Fourier-filtered scale-up of c showing clearly the nonperiodic variation of the contrast, with the inset showing a simulation calculated from the supercell approximation at a thickness of 4.4 nm. The small white rhombus shows the basic unit cell; the large white rhombus shows the unit cell of the supercell approximation.

Our first aim was to understand the diffraction pattern. We have calculated a three-dimensional map of reciprocal-space intensity from the collected series of images. Figure 2 shows views of this map. The reciprocal space is very complicated, but the whole diffraction pattern can be indexed as an incommensurately modulated structure with a hexagonal basic unit cell corresponding to η-Cu_3Si and with two modulation vectors $\mathbf{q}_1 = (\alpha, \alpha, 1/3)$ and $\mathbf{q}_2 = (-2\alpha, \alpha, 1/3)$. These two vectors are related by a three-fold axis. Each spot in the diffraction pattern can thus be indexed with five integers *hklmn*, and the superspace description of the structure requires a five-dimensional superspace. The spots forming hexagons around the main reflections in the zone [001] (Figure 1) can be indexed with $\mathbf{q}_1 - \mathbf{q}_2$ or a symmetry equivalent, and they are thus mixed-order satellites of the type $hkl1\bar{1}$. The value of α was determined from the positions of the spots in the 001 zone axis pattern to be 0.244(1).

Having understood the basic geometry of the diffraction pattern, we processed the data in a way common in X-ray crystallography, which is now becoming popular also in quantitative electron crystallography. A detailed account of a possible approach to automatic data processing of a tilt series of electron diffraction patterns was given by Kolb et al.[42,43] We used a similar approach encoded in our own software. The procedure follows four steps:

- Peak search: strong peaks are located on all images, and their coordinates in reciprocal space are calculated. The instrumental parameters, especially the angle between the rotation axis and the horizontal axis of the diffractometer, were refined by an approach similar to that described by Kolb et al.[43]
- Indexing: The "cloud" of peaks was plotted, and the first estimate of the unit cell was entered "by hand" using a graphical interface in Jana2006.[43]
- Refinement of orientation matrix: The orientation matrix was refined against all peak positions.
- Integration: The orientation matrix obtained in a previous step was used to predict the position of reflections in the images. Peak intensities were located in the vicinity of the predicted positions, and total diffracted intensities were integrated using the standard background−peak−background approach, yielding a reflection list suitable for further processing by crystallographic software. Satellites up to third order were observed in the data set. However, the third order satellites had very weak and inconsistent intensities, and we decided to exclude them from the final data set. Reflections up to $\sin(\theta/\lambda) = 0.7$ were included in the data set.

The deviation of α from 1/4 is small, and the data were therefore indexed and integrated in a $4 \times 4 \times 3$ supercell. This data set was then reindexed to five integer indices on the basis of the basic cell plus two modulation vectors $\mathbf{q}_1$ and $\mathbf{q}_2$.

The description of the details of the complete procedure from diffracted images to the set of integrated diffraction intensities is available as Supporting Information.

STRUCTURE SOLUTION AND REFINEMENT

Symmetry. The diffraction pattern belongs to the Laue class $\bar{3}1m$ (Figure 2b), with $R_{int}(\bar{3}1m) = 16.75\%$. Such an R_{int} would

dx.doi.org/10.1021/ic200102z |*Inorg. Chem.* 2011, 50, 3743–3751

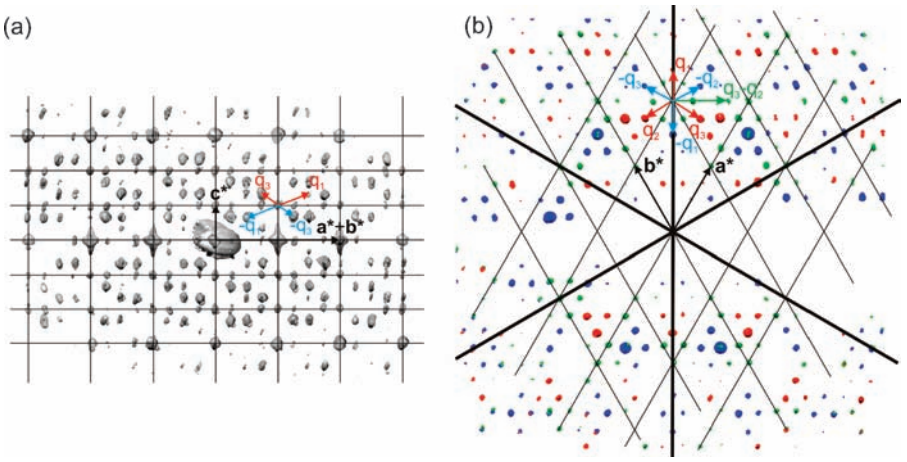

Figure 2. Three-dimensional distribution of diffracted intensities in reciprocal space. (a) Projection along $\mathbf{a}^*-\mathbf{b}^*$ with the basic unit cell and modulation vectors indicated. Vectors $\mathbf{q}_3$ and $-\mathbf{q}_2$ point partly toward the reader (cf. part b of this figure); other vectors lie in the plane of the drawing. (b) Three layers viewed along $\mathbf{c}^*$. Blue, $l = 2/3$; green, $l = 1$; red, $l = 4/3$.

be poor for X-ray diffraction data, but it is very reasonable for electron diffraction data. The diffraction pattern does not contain any trace of systematic absences. Thus, the space group of the average structure is $P\bar{3}1m$, $P31m$, or $P312$, and the symmetry operations of the five-dimensional superspace group do not contain any intrinsic shifts. The superspace group symbol is thus $P\bar{3}1m(\alpha, \alpha, 1/3)000(-2\alpha, \alpha, 1/3)000$ (number 162.2.76.3 in the recently published tables[45]), $P31m(\alpha, \alpha, 1/3)000(-2\alpha, \alpha, 1/3)000$ (SSG number 157.2.83.7), or $P312(\alpha, \alpha, 1/3)000(-2\alpha, \alpha, 1/3)000$ (SSG number 149.2.76.3). The analysis of the structure solution (see below) showed that the structure has the centrosymmetric superspace group $P\bar{3}1m(\alpha, \alpha, 1/3)000(-2\alpha, \alpha, 1/3)000$.

The indexing is most easily understood using modulation vectors with rational component 1/3 along $\mathbf{c}^*$ (Figure 2). However, for the description of the structure in superspace, it is advantageous to transform the modulation vectors to the supercentered setting.[45] In this setting the $\mathbf{q}$ vectors do not contain rational components. This can be achieved by dividing the basic vector $\mathbf{c}^*$ by 3 and introducing appropriate centering in superspace. The centering vectors are $X_1 = (0,0,2/3,1/3,1/3)$ and $X_2 = (0,0,1/3,2/3,2/3)$, and the corresponding reflection condition is $hklmn$: $l - m - n = 3n$. The modulation vectors become $\mathbf{q}_1 = (\alpha, \alpha, 0)$ and $\mathbf{q}_2 = (-2\alpha, \alpha, 0)$. The structure analysis was performed using the supercentered setting of the superspace group, and all subsequent discussion will be based on this setting. For a complete list of the unit cell dimensions, modulation vectors, and symmetry operations, see Table 1.

Structure Solution in Superspace. The structure was solved by charge flipping in superspace[37−39] using the computer program Superflip,[46] assuming kinematical diffraction intensities. The outcome of the charge flipping algorithm is an approximate superspace scattering density. As the charge flipping algorithm does not use explicit information about symmetry, it is possible to obtain symmetry information by analysis of the reconstructed scattering density.[47] This procedure found the superspace group $P\bar{3}1m(\alpha, \alpha, 1/3)000(-2\alpha, \alpha, 1/3)000$, which is in agreement with one of the three superspace groups derived from the symmetry of the diffraction pattern. Consistent results from this symmetry determination and from the analysis of the diffraction pattern give us high confidence that the symmetry has been correctly determined.

Structure Refinement. The refinement of the parameters of a structural model is a standard and routine procedure in X-ray crystallography, where the diffracted intensities are well described by the kinematic model. This model is inappropriate for the diffraction of electrons, and dynamical theory is necessary for the quantitative description of electron diffraction. The precession method[32] is used for structure solution by electron diffraction to make the diffracted intensities less affected by the dynamical effects and to allow the use of kinematic theory for the structure analysis. This approach is very efficient for the solution of structures from electron diffraction.[48−52] However, the dynamical effects are too strong even in PED to allow for a rigorous structure refinement using kinematic theory against PED data. Nevertheless, it is a common practice in the current literature to perform the refinement,[48−52] because there is currently no feasible alternative. The structure refinement based on electron diffraction data rarely improves the model, but the stability of the refinement procedure alone can be understood as a model validation. However, the crystallographic R values of such refinements are typically in the range 25−30%, sometimes more, and only in most favorable cases do they go slightly below 20%. With such high R values, errors in the model cannot be excluded. Moreover, standard uncertainties derived from the least-squares procedure are based on the assumption of independent random errors in the data. This assumption is definitely not fulfilled in the PED data, and thus the structural parameters are very likely to be biased and their error estimates inappropriate.

In the present work, the situation is furthermore complicated by the incommensurate nature of the structure, and by the extreme modulations present in the structure (see below for the description of the modulation functions). The incommensurately modulated structures are usually described in superspace, and the modulation functions of individual atoms are modeled by a continuous function, typically by a Fourier series. However, the modulations in the current structure contain discontinuities and cannot be modeled by simple functions (Figure 4). The number of parameters necessary to model these functions would be prohibitive.

Another option is to approximate the components of the modulation vectors by a rational number. This is equivalent to approximating the nonperiodic modulated structure by a periodic supercell. In the

present case, the modulation vectors have components close to 1/4, and the structure can be approximated in a 4 × 4 supercell with symmetry $P\bar{3}1m$. The initial positions of the atoms in the supercell model were obtained in the following way: The reflections were indexed in the supercell by setting $h_{sc} = 4h + m$, $k_{sc} = 4k + n$, $l_{sc} = l$. These reflections were assigned their phases from the 5D structure solution by charge flipping and a Fourier map calculated. The supercell model was constructed from the peak positions in this Fourier map. The model contains 42 independent Cu atoms and 11 Si/Ge atoms. If all atoms are refined with only isotropic displacement parameters, the model contains 165 parameters. It could be refined against 1185 independent reflections (330 observed with $I > 3\sigma$, and 855 unobserved with $I < 3\sigma$) to residual R values $R_{obs} = 26.15\%$ and $R_{all} = 40.66\%$. It is obvious that the number of parameters is too large for the number of reflections available. This problem resulted also in variable refined isotropic displacement parameters, some of which are very large, and shifts of the atoms in the refined structure that resulted in distorted atomic environments. The too low data-to-parameters ratio and the inappropriateness of the kinematical model for PED data make the refined structure so unreliable that for the interpretation of the structure we decided to use the *ab initio* reconstructed superspace electron density and the supercell model derived directly from the superspace solution. However, the stability of the model in the refinement despite these limitations is a good supplementary indication that the basic features of the model are correct.

RESULTS AND DISCUSSION

η'-Cu_{3+x}(Si,Ge) has a layered structure with layers stacked along **c**. One unit cell contains 18 layers, but due to the centering, the average structure repeats three times in the unit cell. Thus, the average structure contains only six layers. Only four of these six layers are symmetry independent (Figure 3). Each layer contains one symmetry independent atom. Layers A and C, although symmetry independent, are very similar with one atom per basic unit cell and small amplitude of the modulation (Figure 4a,b). Layer B has two atoms per unit cell. These atoms form a honeycomb pattern in the average structure (Figure 3) but also show extremely large modulations (Figure 4c,d). Finally, atoms in layer D also form a honeycomb pattern, but atoms in this layer exhibit quite small modulations. The average structure can be understood as a β-USi_2 structure[53] with uranium atoms replaced by face-sharing Cu clusters in the form of capped hexagonal prisms. It is noteworthy that the atomic positions in the average structure have a symmetry of *P6/mmm*, and it is only the modulation that induces the lower, trigonal symmetry.

The assignment of chemical types to the atomic positions cannot be made directly from the density map. The data quality is not sufficient to rely on the peak height in the density to distinguish between Cu (29 electrons) and a mixed Si/Ge site (23 electrons on average), or to make any conclusions about possible modulation of occupancy of the atoms. However, the symmetry allows only one assignment that leads to an acceptable composition without disorder between Cu and Si/Ge atoms, namely, a Cu atomic type in layers A, B, and C and a mixed Si/Ge occupancy at positions in layer D. The nominal composition of the average structure is $Cu_{3.5}$(Si,Ge).

It is plausible to assume that the average structure of η'-$Cu_{3+x}Si$ corresponds to the structure of the high-temperature phase η-$Cu_{3+x}Si$. However, our average structure is in variance with the previously proposed model for η-$Cu_{3+x}Si$.[22] In this model, the atoms occupy the same positions in the unit cell as in our model, but the two atoms in the honeycomb layers are not symmetry equivalent. Wen and Spaepen proposed a model with alternating Cu and Si atoms in two of the three honeycomb layers. The symmetry of such a model is $P\bar{3}m1$. The symmetry was inferred from small variance of the intensity in the CBED patterns. However, our 3D diffraction data show unambiguously that the point group of the structure is $\bar{3}1m$, which is incompatible with the model proposed by Wen and Spaepen. Mattern et al.[23] propose the same model as Wen and Spaepen on the basis of the high-temperature powder diffraction data of $Cu_{3+x}Si$. However, the powder diffraction pattern of our model and the model by Wen and Mattern are very similar and differ only in the intensities of weak reflections. It is questionable if these two models can be reliably distinguished in the high-temperature powder diffraction pattern. It cannot be excluded that the high-temperature structure of $Cu_{3+x}Si$ corresponds to the model of Wen and Mattern and that it transforms from $P\bar{3}m1$ to $P\bar{3}1m$ upon the phase transition from η to the η' phase. But, we believe it is more likely that the η phase has a structure corresponding to the average structure of the η' phase as defined in this work.

Table 1. Basic Crystallographic Information

basic unit cell	$a = 4.1084(8)$
	$c = 22.228(7)$
modulation vectors	$\mathbf{q}_1 = (\alpha\ \alpha\ 0)$
	$\mathbf{q}_2 = (-2\alpha\ \alpha\ 0)$
	$\alpha = 0.244(1)$
standard superspace group symbol	$P\bar{3}1m(\alpha, \alpha, 1/3)000(-2\alpha, \alpha, 1/3)000$
superspace group symbol in the supercentered setting	$X\bar{3}1m(\alpha, \alpha, 0)000(-2\alpha, \alpha, 0)000$
centering vectors	$X_1 = (0, 0, 2/3, 1/3, 1/3)$
	$X_2 = (0, 0, 1/3, 2/3, 2/3)$
symmetry operators	x1, x2, x3, x4, x5
	−x2, x1−x2, x3, −x4 − x5, x4
	x2, x1, x3, x4, −x4 − x5
	−x1, −x2, −x3, −x4, −x5
	−x1 + x2, −x1, x3, x5, −x4 − x5
	−x1, −x1 + x2, x3, x5, x4
	x2, −x1 + x2, −x3, x4 + x5, −x4
	x1 − x2, −x2, x3, −x4 − x5, x5
	x1 − x2, x1, −x3, −x5, x4 + x5
	−x2, −x1, −x3, −x4, x4 + x5
	x1, x1 − x2, −x3, −x5, −x4
	−x1 + x2, x2, −x3, x4 + x5, −x5

An incommensurately modulated structure is characterized by positions of atoms in the average structure and by the modulation functions of the atomic coordinates. In the current case, the modulation has two independent wave vectors, and the modulation is thus a function of two parameters. The positions of all independent atoms were extracted from the 5D solution by the program EDMA.[54] Figure 4 shows modulation functions of the Cu atoms in layers A and B for illustration. Atoms in layers A, C, and D show moderate modulations without large discontinuities and with maximum amplitudes of 0.130 Å, 0.223 Å, and 0.401 Å, respectively. However, the Cu atoms in layer B exhibit an extreme modulation with the x and y coordinates spanning the full size of the unit cell (Figure 4c,d).

The nature of the modulation is best understood by exploring the real nonperiodic structure. Figure 5 shows a large real-space section of the electron density at the level of layer B. It shows that the Cu atoms are not arranged in a regular honeycomb pattern as in the average structure but form a complicated tiling of the plane consisting mainly of pentagons, accompanied by regular or

dx.doi.org/10.1021/ic200102z |*Inorg. Chem.* 2011, 50, 3743–3751

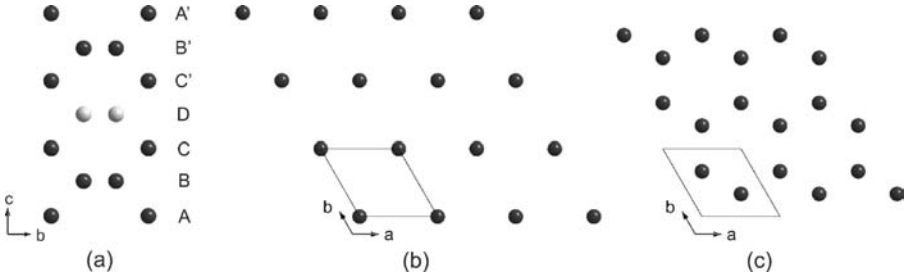

Figure 3. Average structure of η'-$Cu_3(Si,Ge)$. (a) View along [100]. Dark spheres represent Cu; light spheres are Si/Ge mixed sites. Layers labeled with different letters are symmetry-independent; primed labels denote layers related by inversion center. (b) Distribution of atoms in close-packed layers A and C. (c) Distribution of atoms in honeycomb layers B and D.

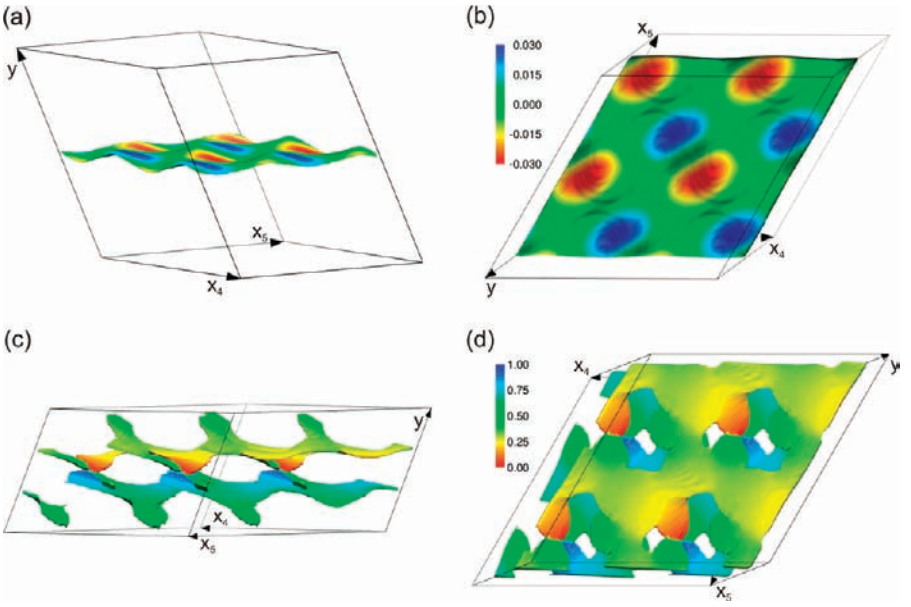

Figure 4. Two views of modulation functions of atoms in layer A (a,b) and B (c,d) in the $x-y$ plane. The surfaces in the images show the y coordinate of the atoms as a function of the modulation phase (denoted x_4, x_5). The color of the surface shows the x coordinate of the atom. Each point on the surface corresponds to one atomic position in the infinite structure. Note the different scale in the color codes. The y coordinate of the Cu atom in images a and b was shifted by 0.5 for clarity of presentation. 2 × 2 unit cells along x_4 and x_5 are shown in c and d for better visualization of the complicated function.

elongated hexagons. The Cu atoms of layers A and C are located above and below each pentagon or hexagon. The modulation of layer B in the $x-y$ plane is the fundamental feature of the structure. Modulations in other layers are much smaller, and their effect is to optimize the interatomic distances to atoms in layer B.

Given the extreme complexity of the modulation of layer B, it would be very difficult to analyze the full modulated structure in detail. The 4 × 4 supercell that was used for the refinement provides a reasonable approximation that captures most of the features of the structure. In the following discussion, we will use this supercell approximation, and at the end, we will point out the main differences between the supercell approximation and the real structure.

The structure consists of five layers of Cu atoms separated by one layer of Si/Ge atoms. The structure can be interpreted as an alternation of the Si/Ge honeycomb layers and slabs of face- or edge-sharing Cu clusters (Figure 6). These clusters contain one Cu atom from layer A in the center and 12−14 Cu atoms coordinating the central atom. Figure 7 shows four basic types of Cu clusters present in the structure. The most frequent cluster is an icosahedral Cu13 cluster (Figure 7a). The second most frequent cluster (Figure 7b) has 11 Cu atoms closely coordinating the central atom at a distance of ca. 2.6 Å and two additional Cu atoms at about 3.3 Å. These clusters will be denoted as 12 + 2 clusters hereafter. One half of the 12 + 2 cluster also corresponds to an icosahedron. The remaining two types of clusters are a capped hexagonal prisms or antiprisms and occur only around Cu atoms at special positions (Figure 7c,d).

The 13-atom icosahedral cluster is found frequently in complex metallic alloys, and it is also reported to be the most stable arrangement of isolated 13 Cu atoms.[55] η'-$Cu_{3+x}Si$ shows a remarkable interplay between the striving of the Cu atoms for locally energetically advantageous configuration, which is an icosahedral cluster, and a long-range periodicity. The separating layers of Si atoms play a crucial role in the stabilization of the structure. They define two-dimensional Cu slabs, which can develop modulation that is not observed in bulk copper, but also impose periodicity and trigonal symmetry on the structure, so that the final structure, despite the strong modulations, remains on average periodic.

dx.doi.org/10.1021/ic200102z |*Inorg. Chem.* 2011, 50, 3743–3751

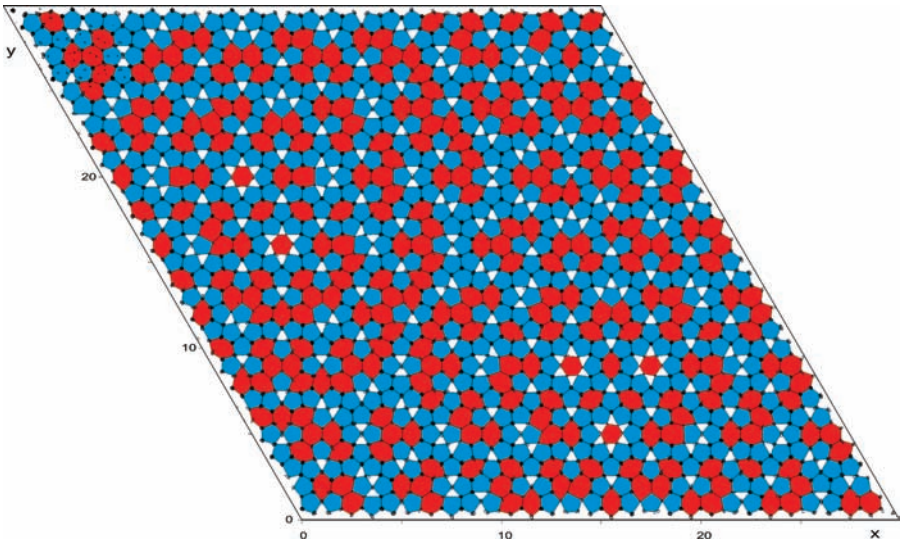

Figure 5. Real-space section through the electron density at the level of layer B. Each black spot in the image corresponds to one peak in the density map. Blue pentagons and red hexagons were added to better visualize the tiling of the plane. Although in most cases the distinction between a pentagon and an elongated hexagon is unambiguous, transitional forms between the two extremes also occur. Low-density noise was deleted for clarity. The original unmodified density is shown in the upper left corner of the image.

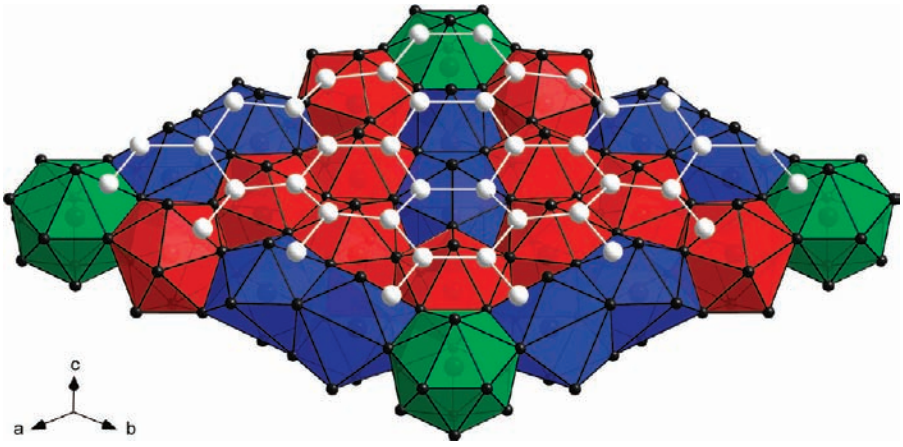

Figure 6. Structure in the supercell approximation showing one slab of Cu clusters and one layer of Si/Ge atoms. The clusters are colored according to Figure 7.

The replacement of hexagonal capped prisms of the average structure by the icosahedra and 12 + 2 clusters also has implications for the stoichiometry of the structure. Instead of 192 Cu atoms in layer B per 48 unit cells of the average structure, the superstructure contains only 176 atoms. The formula of such a structure is $Cu_{3.333}Si$, or 76.9 atom % Cu in the alloy. This coresponds within experimental error to the composition determined by EDS. It also almost exactly corresponds to the Cu-rich edge of the stability range of the η'-$Cu_{3+x}Si$.[56] A further reduction in Cu content necessary to explain Si-richer η'-$Cu_{3+x}Si$ can be explained either by having a slightly different shape of the modulation function combined with a modified modulation wave vector or by assuming partial vacancies in the centers of Cu clusters with most unfavorable coordinations. The former explanation is indirectly supported by the observation by Wen and Spaepen, who observed a variation of the wave vector component between 0.266 and 0.289.

One unit cell of the supercell approximation contains 27 icosahedral clusters, 18 clusters of the 12 + 2 type, and three hexagonal capped prisms or antiprisms. The latter clusters appear only around central atoms in special positions, which are artificially generated by the supercell approximation. These highly symmetric positions occur with much lower frequency in the true structure.

As an independent means of validating the structure solution, we have calculated a multislice simulation of a HRTEM image from the supercell approximation and compared it with the experimental image (Figure 1) using the computer program JEMS.[57] The best fit was obtained with a thickness of two unit cells (4.4 nm). The simulation reproduces the main features of the experimental image quite well, especially the overall honeycomb pattern in the image. The honeycomb pattern might seem surprising given the strong modulation of layer B, but note that each unit cell contains six layers B, each with different phase of the modulation. A projection along $\mathbf{c}^*$ of two unit cells thus averages out a large part of the modulation of the B layer. While the overall appearance of the multislice simulation is correct, the

dx.doi.org/10.1021/ic200102z |*Inorg. Chem.* 2011, 50, 3743–3751

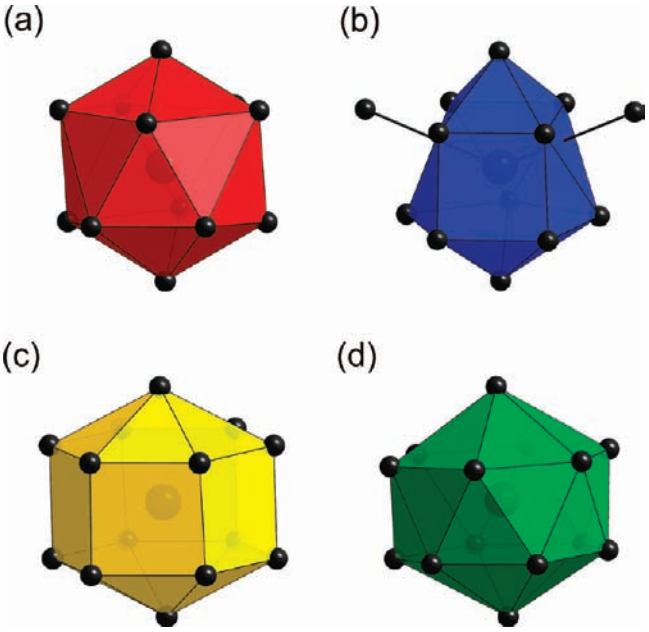

Figure 7. Typical clusters found in the supercell structure with layer A atoms in the center. (a) Icosahedron, (b) the 12 + 2 cluster, (c) hexagonal capped prism, (d) hexagonal capped antiprism.

details do not match the experiment perfectly. Most notably, the simulation shows motifs at the edges of the unit cell that are not found in the experimental image. These motifs are artifacts of the supercell approximation and demonstrate that even the relatively large 4 × 4 supercell is not sufficient to capture all features of the modulated structure faithfully. Moreover, the simulation was based on a structure, where each Si/Ge position is occupied with a hypothetical mixed Si/Ge atom, while in reality the Si and Ge atoms are randomly distributed. Furthermore, in very thin samples, surface relaxation effects can play an important role and alter the local structure.

It is notable that we observed the metastable phase η'-$Cu_{3+x}Si$ phase rather than the η''-$Cu_{3+x}Si$ phase, which is reported to be stable at room temperature. We observe the metastable phase despite the fact that the samples were not quenched, but slowly cooled down from 500 °C to room temperature at a rate of approximately 4 K per minute. It is reported[22] that the $Cu_{3+x}Si$ precipitates in silicon are found in this metastable state, but our sample is not embedded in the substrate. A possible explanation is that the admixture of germanium stabilizes the η'-$Cu_{3+x}Si$ phase at room temperature.

CONCLUSIONS

η'-$Cu_{3+x}Si$ has eluded correct structural description for decades due to the combination of a complex, two-dimensional incommensurately modulated structure and difficulty in obtaining large samples suitable for single crystal analysis. All previous studies involved powder samples, thin films on a substrate, or precipitates in a silicon substrate. A recent synthetic technique using the CVD method yielded a material with composition η'-Cu_{3+x}(Si,Ge) in the form of small isolated platelets about 40-nm-thick that were suitable for analysis by 3D quantitative electron diffraction. The analysis suggests that the substitution of germanium for part of the silicon atoms stabilizes the metastable η'-$Cu_{3+x}Si$ phase at room temperature. structure is formed by slabs of Cu clusters separated by monatomic layers of Si and Ge atoms. The Cu slabs are strongly modulated, leading to a predominant icosahedral coordination of the central Cu atoms. The two-dimensional modulation functions describing the shifts of the atoms show an unprecedented complexity and large amplitude. Nevertheless, the resulting structure model exhibits a surprising consistency and elegance. The conflict between the striving for locally favorable icosahedral coordination of the Cu atoms and the need for a long-period arrangement is the most likely reason for the modulation.

This work illustrates the potential of combining three emerging techniques: quantitative 3D diffraction tomography, precession electron diffraction, and *ab initio* phasing by charge flipping. Without the combination of these three methods, the solution of the η'-$Cu_{3+x}Si$ structure would be extremely hard, if not impossible. The technique applied in this work has the potential of making the solution of similar complex structures from nanocrystals almost routine, and it thus opens new perspectives in the structural investigations of metallic alloys and other complex structures from micro- and nanocrystals.

ASSOCIATED CONTENT

Supporting Information. Details of the data processing procedure, list of phased structure factors obtained by *ab initio* phasing by charge flipping, CIF file with the atomic coordinates of the supercell approximation, and tables with modulated positions of individual atoms as function of the modulation phase. This material is available free of charge via the Internet at http://pubs.acs.org/.

AUTHOR INFORMATION

Corresponding Author
*E-mail: palat@fzu.cz.

ACKNOWLEDGMENT

This research was supported by the Grant Agency of the Czech Republic under project no. 203/09/1088 and by the Ministry of Education of the Czech Republic under project no. AVOZ40320502. This work has also been supported by the Praemium Academiae of the Academy of Sciences of the Czech Republic.

REFERENCES

(1) Weber, T.; Dshemuchadse, J.; Kobas, M.; Conrad, M.; Harbrecht, B.; Steurer, W. *Acta Crystallogr., Sect. B* **2009**, *65*, 308–317.
(2) Steurer, W.; Deloudi, S. *Crystallography of Quasicrystals: Concepts, Methods and Structures*; Springer: New York, 2009; Springer Series in Materials Science, Vol. 126.
(3) Bernard, F.; Souha, H.; Gaffet, E. *Mater. Sci. Eng., A* **2000**, *284*, 301–306.
(4) Aboelfotoh, O. M.; Krusin-Elbaum, L. *J. Appl. Phys.* **1991**, *70*, 3382–3384.
(5) An, Z.; Ohi, A.; Hirai, M.; Kusaka, M.; Iwami, M. *Surf. Sci.* **2001**, *493*, 182–187.
(6) Stolt, L.; Charai, A.; Dt'Heurle, M. F.; Fryer, M. P.; Harper, J. M. E. *J. Vac. Sci. Technol. A* **1991**, *9*, 1501–1505.
(7) Aboelfotoh, O. M.; Borek, A. M.; Narayan, J. *Appl. Phys. Lett.* **1999**, *75*, 1739–1741.

(8) Darling, A. K.; Guduru, K. R.; Reynolds, L. C., Jr; Bhosle, M. V.; Chan, N. R.; Scattergood, O. R.; Koch, C. C.; Narayan, J.; Aboelfotoh, O. M. *Intermetallics* **2008**, *16*, 378–383.
(9) Liu, S. C.; Chen, J. L. *Thin Solid Films* **1995**, *262*, 187–198.
(10) Liang, H. H.; Luo, S. J.; Lin, T. W. *Mater. Sci. Semicon. Proc.* **2001**, *4*, 233–235.
(11) Liang, H. H.; Luo, S. J.; Lin, T. W. *Micron* **2002**, *33*, 561–564.
(12) Lin, T. C.; Lin, L. K. *Mater. Chem. Phys.* **2003**, *82*, 306–315.
(13) Zhang, Z.; Wong, M. L.; Ong, G. H.; Wang, J. X.; Wang, L. J.; Wang, S. J.; Chen, H.; Wu, T. *Nano Lett.* **2008**, *8*, 3205–3210.
(14) Li, S.; Cai, H.; Gan, C. L.; Guo, J.; Dong, Z.; Ma, J. *Cryst. Growth Des.* **2010**, *10*, 2983−2989.
(15) Panin, V. A.; Shugurov, R. A.; Ivonin, V. I.; Shesterikov, V. Ye. *Semiconductors* **2010**, *44*, 116–122.
(16) Wen, Y. C.; Reuter, C. M.; Tersoff, J.; Stach, A. E.; Ross, M. F *Nano Lett.* **2010**, *10*, 514–519.
(17) Echigoya, J.; Enoki, H.; Satoh, T.; Waki, T.; Ohmi, T.; Otsuki, M.; Shibata, T. *Appl. Surf. Sci.* **1992**, *56*−*58*, 463–468.
(18) Wampler, R. W. *Mater. Res. Soc. Symp. Proc.* **1997**, *448*, 371–376.
(19) Chen, J. L.; Liu, S. C.; Lai, B. J. *Mater. Sci. Semicon. Proc.* **2004**, *7*, 143–156.
(20) Arrhenius, S.; Westgren, A. *Z. Phys. Chem. Abt. B* **1931**, *14*, 66–79.
(21) Solberg, K. J. *Acta Crystallogr.* **1978**, *A34*, 684–698.
(22) Wen, Y. C.; Spaepen, F. *Philos. Mag.* **2007**, *87*, 5581–5599.
(23) Mattern, N.; Seyrich, R.; Wilde, L.; Baehtz, C.; Knapp, M.; Acker, J. *J. Alloy Compd.* **2007**, *429*, 211–215.
(24) Schubert, K.; Brandauer, G. *Z. Metallkd.* **1952**, *43*, 262–268.
(25) Huaiying, Z. *J. Less-Common. Met.* **1991**, *171*, 113–118.
(26) Nowotny, H.; Bachmayer, K. *Monatsh. Chem.* **1950**, *81*, 669–678.
(27) Krusin-Elbaum, L.; Aboelfotoh, O. M. *Appl. Phys. Lett.* **1991**, *58*, 1341–1343.
(28) Wagner, T.; Schoenleber, A. *Acta Crystallogr., Sect. B* **2009**, *65*, 249–268.
(29) van Smaalen, S. *Incommensurate Crystallography*; Oxford University Press: New York, 2007.
(30) Kolb, U.; Gorelik, T.; Kuebel, C.; Otten, M. T.; Hubert, D. *Ultramicroscopy* **2007**, *107*, 507–513.
(31) Zhang, D.; Oleynikov, P.; Hovmoller, S.; Zou, X. *Z. Krist.* **2010**, *225*, 94−102.
(32) Vincent, R.; Midgley, P. A. *Ultramicroscopy* **1994**, *53*, 271–282.
(33) Own, C. S.; Marks, L. D.; Sinkler, W. *Acta Crystallogr., Sect. A* **2006**, *62*, 434–443.
(34) Ciston, J.; Deng, B.; Marks, L. D.; Own, C. S.; Sinkler, W. *Ultramicroscopy* **2008**, *108*, 514–522.
(35) White, T. A.; Eggeman, A. S.; Midgley, P. A. *Ultramicroscopy* **2010**, *110*, 763–770.
(36) Eggeman, A. S.; White, T. A.; Midgley, P. A. *Ultramicroscopy* **2010**, *110*, 771–777.
(37) Oszlányi, G.; Sütő, A. *Acta Crystallogr., Sect. A* **2004**, *60*, 134–141.
(38) Oszlányi, G.; Sütő, A. *Acta Crystallogr., Sect. A* **2008**, *64*, 123–134.
(39) Palatinus, L. *Acta Crystallogr., Sect. A* **2004**, *60*, 604–610.
(40) Mugnaioli, E.; Gorelik, T.; Kolb, U. *Ultramicroscopy* **2009**, *109*, 758–765.
(41) Eggeman, A.; White, T.; Midgley, P. *Acta Crystallogr., Sect. A* **2009**, *65*, 120–127.
(42) Kolb, U.; Gorelik, T.; Otten, M. T. *Ultramicroscopy* **2008**, *108*, 763–772.
(43) Kolb, U.; Gorelik, T.; Mugnaioli, E. *Mater. Res. Soc. Symp. Proc.* **2009**, *1184*, Warrendale PA, USA, GG01-05.
(44) Petříček, V.; Dušek, M.; Palatinus, L. *The Crystallographic Computing System JANA2006*; Institute of Physics: Praha, Czech Republic, 2006.
(45) Stokes, H. T.; Campbell, B. J.; van Smaalen, S. *Acta Crystallogr., Sect. A* **2011**, *67*, 45–55.
(46) Palatinus, L.; Chapuis, G. *J. Appl. Crystallogr.* **2007**, *40*, 786–790.
(47) Palatinus, L.; van der Lee, A. *J. Appl. Crystallogr.* **2008**, *41*, 975–984.
(48) Hadermann, J.; Abakumov, A. M.; Tsirlin, A. A.; Filonenko, V. P.; Gonnissen, J.; Tan, H.; Verbeeck, J.; Gemmi, M.; Antipov, E. V.; Rosner, H. *Ultramicroscopy* **2010**, *110*, 881–890.
(49) Gemmi, M.; Klein, H.; Rageau, A.; Strobel, P.; Le Cras, F. *Acta Crystallogr.* **2010**, *B66*, 60–68.
(50) Rozhdestvenskaya, I.; Mugnaioli, E.; Czank, M.; Depmeier, W.; Kolb, U.; Reinholdt, A.; Weirich, T. *Mineral. Mag.* **2010**, *74*, 159–177.
(51) White, T. A.; Sergio Moreno, M.; Midgley, P. A. *Z. Kristallogr.* **2010**, *225*, 56–66.
(52) Birkel, C. S.; Mugnaioli, E.; Gorelik, T.; Kolb, U.; Panthoefer, M.; Tremel, W. *J. Am. Chem. Soc.* **2010**, *132*, 9881–9889.
(53) Zachariasen, W. H. *Acta Crytsallogr.* **1949**, *1*, 94–99.
(54) van Smaalen, S.; Palatinus, L.; Schneider, M. *Acta Crystallogr., Sect. A* **2003**, *59*, 459–469.
(55) Mazalova, V. L.; Soldatov, V. *J. Struct. Chem.* **2008**, *49*, S107–S115.
(56) Massalski, T. B. *Binary Alloys Phase Diagrams, Vol. 1 Ac-Au to Fe-Rh*; ASM: Metal Park, OH, 1986; pp 960−961.
(57) Stadelmann, P. *JEMS, Electron Microscopy Software*; CIME-EPFL: Lausanne, Switzerland, 2004.